Electron pairing instabilities and magnetic properties in nanoclusters and nanomaterials

A.N. Kocharian*, G.W. Fernando**, Kun Fang** and K. Palandage***

* California State University, Los Angeles, CA, USA, armen.kocharian@calstatela.edu
** Department of Physics, University of Connecticut, Storrs, CT, USA
*** Department of Physics, Trinity College, Hartford, CT, USA

ABSTRACT

Studies of assembled clusters, nanoparticles in various topologies provide intriguing insights into several many body problems in condensed matter physics. A new, emerging guiding principle for the search of new materials can be identified as spatial inhomogeneities and density phase separation instabilities in the proximity to quantum critical points (QCPs). Electron coherent and incoherent pairings and formation of various types of magnetic correlations in different bipartite and frustrated geometries are studied under variation of interaction strength, electron doping, inter-site coupling and temperature. The exact calculations of charge and spin phase separation, collective excitations and pseudogaps yield level crossing phase separation instabilities, Mott-Hubbard localization and ferromagnetism, Bose-Einstein condensation and possible superconductivity. Criteria are found for quantum melting of the Mott-Hubbard and antiferromagnetic insulators into the charge and spin liquids driven by interaction strength, next nearest coupling and temperature. Resulting phase diagrams resemble a number of inhomogeneous, coherent and incoherent nanoscale phases seen in high Tc cuprates, pnictides and manganites nanomaterials. The relationship of these results to superconductivity and ferromagnetism in larger size systems is discussed.

Keywords: high T_c superconductivity, inhomogeneities, phase separation, charge pairing, spin pairing, ferromagnetism, full Bose condensation, quantum melting

1 Introduction

A key element for understanding the complexity and perplexity in high-Tc cuprates, pnictides chalcogenides and manganites nanomaterials is the experimental observation of phase separation (PS) instabilities at the nanoscale signaled by electron phase separation PS instabilities [1]–[4]. A new guiding principle for the search of new nanomaterials with enhanced Tc is the proximity to the quantum critical points (QCPs) for spontaneous first order QPTs attributed to intrinsic spatial inhomogeneities [5]–[9]. The inhomogeneous concentrated system in equilibrium can be approximated as a quantum gas of decoupled clusters, which do not interact directly but through thermal reservoir by allowing the energy and electron number to fluctuate. Our results for possible spatial inhomogeneities are directly applicable to nanosystems which usually contain an immense number of isolated clusters in contact with a thermal reservoir by allowing electron number per cluster to fluctuate. The finite-size optimized clusters may be one of the few solid grounds available to handle this challenging problem by defining canonical and the grand canonical local gap order parameters in the absence of long-range order [10]. The PS instabilities and spin-charge separation effects in bipartite Hubbard clusters driven by onsite Coulomb interaction U display QCPs which strongly depend on cluster topology [11]–[13]. In frustrated (nonbipartite) geometries spontaneous transitions depend on the sign of the coupling t and can occur for all U by avoiding QCPs (level crossings) at finite U values. The existence of the intrinsic QCPs and inhomogeneities associated with PS instabilities, are crucial ingredients of the superconducting (SC) and ferromagnetic (FM) QPTs, providing important clues for understanding the incipient microscopic mechanisms of pairing instabilities in real space due to coexisting high/low electron (hole) or high/low spin up (down) densities in SC and FM nanomaterials respectively. However, small systems suffer from finite-size (edge) effects, so it is unclear whether the observed instabilities can survive in the thermodynamic limit. Thus, tests on reduced boundary effects are necessary to confirm the picture of local instabilities in larger systems in the so-called "optimized" Betts finite square lattices [14]–[18]. The Betts unit cells are taking full advantage of the local space group symmetries of the original isotropic 2d (square) bipartite lattice.

2 Model and Methodology

We consider the minimal Hubbard model with the nearest (nn) and next-nearest-neighbors (nnn):

$$H = -t \sum_{\langle i,j\rangle\ \sigma} c^{+}_{i\sigma}\, c_{j\sigma} - t' \sum_{\langle\langle i,j\rangle\rangle\ \sigma} c^{+}_{i\sigma}\, c_{j\sigma} + U \sum_{i} n_{i\uparrow} n_{i\downarrow} \quad (1)$$

where summation over i and j in Eq. (1) goes through all lattice sites L with coupling integral t for the nearest neighbors and next nearest neighbors, $t_{nnn} = t'$ and $U > 0$ is the on-site Coulomb interaction.

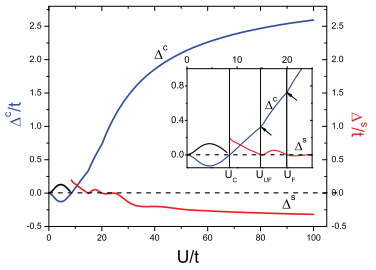

Figure 1: Δ^c, Δ^s and Δ^h gapa in 8-site Betts lattice as a function of U at $T = 0$ and $N = 7$. When $U < 8.52$, the negative charge gap ($\Delta^c < 0$) with paired ($\uparrow\downarrow$) spins implies a coherent hole-hole pairing with $\Delta^c = -\Delta^h$. As $U > 8.52$, the positive charge gap $\Delta^c > 0$ provides stability for electron-hole pairing, while zero $\Delta^h = 0$ is referring to a gapless excitation.

2.1 Phase separation instabilities

An exact diagonalization technique is used to extract the pairing instabilities and QCPs in finite 2d square lattices generated by small Betts unit cells. In our previous work (Refs [11]–[13]), we have discussed PS instabilities in selected cluster geometries. A collection of "clusters" can be treated at a fixed average number of electrons $\langle N\rangle$ and total spin $\langle S\rangle$ in a canonical ensemble. We define a charge Δ^c gap as $\Delta^c = E(N+1,T) + E(N-1,T) - 2E(N,T)$ and spin gap, $\Delta^s = E(N,S',T) - E(N,S,T)$ using canonical energies $E(N,S,T)$ at a given U and temperature T. The negative charge and spin gaps at $T = 0$ for different U values display corresponding PS instabilities (Fig. 1). The PS near half filling is strongly dependent on the lattice geometry (topology) and also signs of t and t' coupling terms.

2.1.1 Quantum critical points

As temperature approaches zero ($T \to 0$), the possible sign change in canonical gaps signifies the existence of QCPs related to first order (dramatic) changes. The nodes of the charge and spin gaps, defined by $\Delta^{c,s}(U) = 0$, are the QCPs for the onset of charge and spin PS and the corresponding charge and spin density inhomogeneities due to spontaneous redistribution of the charge and spin liquids among the clusters. The nodes of the charge gap, at which charge gap disappears ($\Delta^c(U_c) = 0$) defines the quantum critical point $U_c = 8.52$ for the energy level crossings. There is a quantum critical point around $U_s = 14.8$ where the spin gap vanishes, i.e., $\Delta^s(U_s) = 0$ (see inset in Fig. 1). As $8.52 < U < 14.8$, a low total spin is preferable, $S = 0$. As $U > 14.8$, some paired spins tend to be aligned at low temperatures.

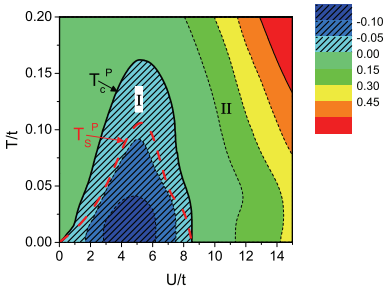

Figure 2: A contour plot of Δ^c versus U and T at $\langle N\rangle$=7. The solid contour denotes a smooth transition at $T_c^P(U)$, $\Delta^c(U, T_c^P) = 0$. Phase I a shaded area describes spontaneous PS instabilities and charge pairing ($\Delta^c < 0$). Phase II without a shaded pattern is the stable MH insulator region ($\Delta^c > 0$). The broken line for onset of coherent pair condensation of $\uparrow\downarrow$ spins at $T_s^P(U)$. Below $T_s^P(U)$ the paired ($\uparrow\downarrow$) spin stiffness of bound charge describes coherent pairing phase with full BEC and superconductivity, while above $T_s^P(U)$ preformed pairs with unpaired spins are incoherent.

This phase diagram displays the main phases found earlier for elementary square geometry in Ref. [11]. Phase I is an hole-hole pairing phase with a negative charge gap and positive spin gap of equal amplitudes ($\Delta^c = -\Delta^h$) at all $U < U_c$. This singlet ($\uparrow\downarrow$) type pairing is similar to the BCS coupling with a single quasiparticle gap we identified as coherent pairing. However, at $T \neq 0$ the charge gap significantly differs from the spin gap. This picture with electron charge pairing and opposite ($\uparrow\downarrow$) spin coupling ($\uparrow\downarrow$) can lead, at low temperatures, to coherent pairings of charge and spin degrees and possible superconductivity (SC). However, this route with two critical T_c^P and T_s^P condensation temperatures in charge and spin channels for possible superconductivity differs from the conventional BCS scenario with a single critical temperature T_c. Phase II is a spin liquid phase with gapless, low spin-$\frac{3}{2}$ excitations. In Phase III, the negative spin gap describes consequent transitions into low spin-$\frac{5}{2}$ (unsaturated) FM states. When U is large enough (not shown), the ground state displays a fully saturated spin-$\frac{7}{2}$ ferromagnetism. In the negative charge gap region ($\Delta^c < 0$), the spin pseudogap is positive, i.e., $\Delta^h > 0$, since in the grand canonical ensemble we define it as the separation between the two consecutive peak positions of magnetic susceptibility χ_h for a given μ near vicinity of QCP, μ_c. Analogously the charge pseudogap Δ^μ in the range of instability $\Delta^c < 0$ at $U \leq U_c$ describes a metallic behavior with the gapless charge excitations, $\Delta^\mu \to 0$. At $U \geq U_c$, the pseudogap, $\Delta^\mu = \Delta^c \geq 0$, increases with U monotonously. Such behavior implies a phase transition from a quantum cold charge liquid state into the Mott-Hubbard insulator at

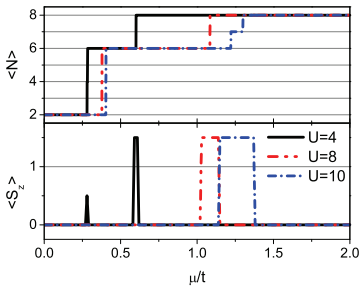

Figure 3: Average $\langle N\rangle$ and $\langle S^z\rangle$ at different U calculated in the grand canonical ensemble at $T = 0$ and small $h = 0.001$. When $U \leq U_c = 8.52$, $\langle N\rangle$ jumps directly from $\langle N\rangle = 6$ to $\langle N\rangle = 8$, which displays electron pairing instability in the charge channel. At large $U = 10$ and $\langle N\rangle$=7 an unpaired spin with $\langle S_z\rangle = \frac{3}{2}$ describes a spin liquid behavior, $\Delta^h = 0$.

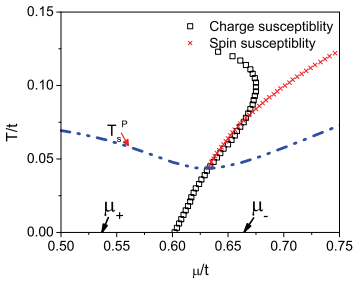

Figure 4: Charge and spin susceptibility peaks near the critical μ_0 for the transition from $N = 6$ to $N = 8$ vs temperature at $U = 4$ and $h \to 0$. Spin susceptibility vanishes below a certain temperature T_s^P, which points to gapless spin excitations.

isolated QCP, U_c. Accordingly, we find that the spin pseudogap vanishes ($\Delta^h \to 0$) in the spin instability region (everywhere at $U > U_c$, where $\Delta^s < 0$). Thus, the isolated QCP, U_c, signifies also a cold quantum melting of antiparallel spin-insulator, $\Delta^h > 0$, for transition into a degenerate spin-liquid without rigidity $\Delta^h \to 0$. At $T \neq 0$ a contour plot of the charge gap at different U and T for $N = 7$ is shown in Fig. 2, where T_c^P and T_s^P are corresponding temperatures for a vanishing charge and spin gaps.

2.1.2 Charge and spin pseudogaps

We study also the charge and spin susceptibilities in the grand canonical ensemble at a fixed chemical potential μ and magnetic h respectively. Fig. 3 shows average electrons number $\langle N\rangle$ and spin $\langle S^z\rangle$ as a function of μ

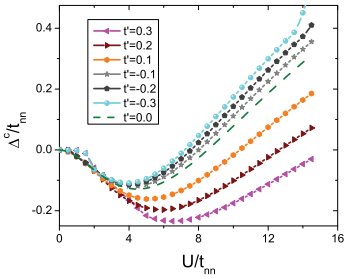

Figure 5: The charge gap Δ^c versus U at various t_{nnn} at $T = 0$. As t_{nnn} >0 increases the crossover point shifts to a larger U value. In contrast, the charge pairing region decreases gradually with $t_{nnn} < 0$, while for $t_{nnn} < 0$ it increases.

at selected U values. The visible plateau near N=7 for $\Delta^c > 0$ at $U = 10$ describes the rigidity of the MH insulating charge gap. We introduce the grand canonical charge pseudogap as a peak-to-peak distance between two consecutive peak positions in charge susceptibility, $\chi_\mu = \frac{\partial N(\mu)}{\partial \mu}$. Correspondingly, we can analyze the variation of the spin $S^z(\mu)$ and susceptibility $\chi_h = \frac{\partial S^z(\mu)}{\partial h}$ as a function of magnetic field h near the critical, μ_c, close to given average electron number, $\langle N\rangle$. In addition, we introduced the grand canonical charge (positive) pseudogap $\Delta^\mu > 0$ as a peak-to-peak distance between two consecutive peak positions of charge susceptibility, χ_μ. A key element for the understanding of various electron instabilities is the exact relationship between the charge and spin Δ^c, Δ^μ gaps and their corresponding counterpart, $\Delta^\mu \geq 0$, $\Delta^h \geq 0$ pseudogaps. At $T \neq 0$ the the charge χ_μ and spin χ_h susceptibility peaks point to gapless spin excitations in Fig. 4.

2.2 Effects of next nearest neighbor hopping

In this section, effects of lattice (non-bipartite) frustrations due to a nonzero t_{nnn} are discussed. The lattice frustration with $t_{nnn} \neq 0$ allows study of electron pairing in the absence of electron-hole symmetry. The positive $t_{nnn} > 0$ provokes electron delocalization and makes the mixed (phase separated) state for electron pairing energetically more favorable (Fig. 5). We found systematic enhancement of coherent pairing by optimization of the t_{nnn} coupling parameter [20]. Magnetic field fluctuations lead to segregation of clusters into regions rich in spin ↑ and spin ↓, i.e., formation of magnetic domains at $t_{nnn} < 0$ in Fig. 6 consistent with the saturated Nagaoka-like FM in large size lattices [19].

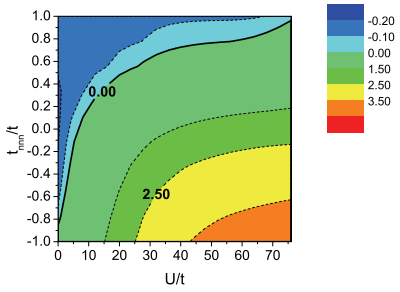

Figure 6: The contour plot of charge gap Δ^c for different U and t_{nnn} at $T = 0$. As $t_{nnn} > 0$ increases the crossover point (solid curve) shifts to a larger U value. In contrast, the charge pairing region decreases with $t_{nnn} < 0$.

3 Conclusion

Exact calculations of critical instabilities performed in the 2d lattices generated Betts unit cells near half filling reproduce the general features found in ensemble of generic small 2×2 and 2×4 lattices [6]–[9]. This behavior is different from that observed in the asymmetric ladder structures where a spontaneous anisotropy leads to an oscillatory behavior of the charge gap in the intermediate U region. Meanwhile, the reduced, minimal-size Betts cells (optimized isotropy in both directions) can still take advantage of the symmetries of the full square lattice and, therefore, can partially restore the bipartite square (C_4) symmetry. In addition, the t_{nnn} term can shift the QCPs and change the gap value and bring to the systematic enhancement of coherent pairing by optimization of t_{nnn} parameter. We find that one can produce electronic and magnetic instabilities in correlated nanomaterials by tuning also intra-coupling in various topologies [11]–[13]. Exact calculations provide a tool for unveiling hidden generic QCPs of PS, hot and cold localization and melting of charge and spin entities. The generated lattices using Betts cells provide a rich playground for understanding of PS instabilities, the fundamentals in superconductivity and magnetism in high Tc cuprates, pnictides, transition metal oxides, manganites, etc., by advancing the prospects for wide technological applications in the nanoscience by synthesizing nanomaterials with unique properties. Building blocks spontaneously organized into ordered structures suggest a bottom-up key paradigm to control QCPs and fabricate of novel assembled nanostructures with new FM and SC properties.

4 Acknowledgments

We acknowledge the computing facilities provided by the Center for Functional Nanomaterials, BNL, which is supported by the U.S. Department of Energy, Office of Basic Energy Sciences, under Contract No.DE-AC02-98CH10886. The work was performed also, in part, at the Center for Integrated Nanotechnologies, a U.S. Department of Energy, Office of Basic Energy Sciences user facility at LANL (Contract DE-AC52- 06NA25396) and Sandia National Laboratories (Contract DE-AC04-94AL85000).

REFERENCES

[1] P. W. Anderson, Science, 235, 1196, 1987.
[2] J. M. Tranquada *et al.*, Nature, 375, 561, 1995.
[3] Y Kohsaka *et al.*, Sience, 315, 1380, 2007
[4] E. Dagotto, Science, 309, 257, 2005; Phys. Rev. Lett. 64, 475, 1990.
[5] A. N. Kocharian, G. W. Fernando, and C. Yang, Spin and charge pairing instabilities in nanoclusters and nanomaterials, In Scanning Probe Microscopy in Nanoscience and Nanotechnology, Edited by B. Bhushan, Springer, pp. 507-570, 2010.
[6] A. N. Kocharian, G. W. Fernando, K. Palandage and J. W. Davenport, J. Magn. Magn. Mater. 300, e585, 2006.
[7] A. N. Kocharian, G. W. Fernando, K. Palandage, and J. W. Davenport, Phys. Rev. B 74, 024511, 2006.
[8] G. W. Fernando, A. N. Kocharian, K. Palandage, T. Wang, and J. W. Davenport, Phys. Rev. B 75, 085109, 2007.
[9] A. N. Kocharian, G. W. Fernando, K. Palandage, T. Wang, and J. W. Davenport, Phys. Lett. A 364, 57, 2007.
[10] S. Sachdev, Science, 288, 475, 2000.
[11] A. N. Kocharian, G. W. Fernando, K. Palandage, and J. W. Davenport, Phys. Rev. B 78, 075431, 2008.
[12] A. N. Kocharian, G. W. Fernando, K. Palandage, and J. W. Davenport, Phys. Lett. A 373, 1074, 2009.
[13] G. W. Fernando, A. N. Kocharian, K. Palandage, and J. W. Davenport, Phys. Rev. B 80, 014525, 2009.
[14] J. Oitmaa, and D.D. Betts, Can. J. Phys. 56, 897, 1978.
[15] D. Betts, H. Lin, and J. Flynn, Can. J. Phys. 77, 353, 1999.
[16] D. D. Betts, S. Masui, N. Vats, and G. E. Stewart, Can. J. Phys. 74, 54, 1996.
[17] E. Kaxiras, and E. Manousakis, Phys. Rev., B 37, 656, 1988.
[18] E. Kaxiras, and E. Manousakis, Phys. Rev. B 38, 866, 1988.
[19] Y. Nagaoka, Phys. Rev. 147, 392, 1966.
[20] K. Fang, G.W. Fernando, A.N. Kocharian, Phys. Lett. A 376, 538, 2012.